TÜBİTAK

Turkish Journal of Earth Sciences

http://journals.tubitak.gov.tr/earth/

Research Article

Turkish J Earth Sci
(2024) 33:
© TÜBİTAK
doi:/yer-2307-9

Anomalous crustal structure beneath the Örenli-Eğiller depression zone, inferred from magnetotelluric studies, Western Anatolia, Türkiye

Dornadula CHANDRASEKHARAM[1,*], Khasi RAJU[2], Prabhala Bhaskhara Venkata Subba Rao[3], Alper Baba[1]

[1]Department of International Water Resources, İzmir Institute of Technology, İzmir, Turkiye
[2]Department of Earth and Geoenvironmental Sciences, University of Bari Aldo Moro, Bari, Italy
[3]Indian Institute of Geomagnetism, Mumbai, India

Received: 10.07.2023 • **Accepted/Published Online:** 04.09.2024 • **Final Version:** 00.00.2024

Abstract: In Türkiye, the prevalence of high radiogenic granites makes them ideal locations for initiating enhanced geothermal system (EGS) projects. One such occurrence of these granites is observed in the Kozak area of the Bergama region. To assess the energy potential of this site, a magnetotelluric (MT) survey was conducted, focusing on determining the depth distribution of the intrusive granite.
The survey employed dimensionality analysis, utilizing Bahr skew and phase tensor analyses that denote a 2D subsurface nature up to 100 s and beyond that a 3D nature. In the present study, we interpreted MT data up to 100 s. The data collected, including rotated impedance tensors and tippers, were inverted using a nonlinear conjugate gradient algorithm integrated into the MT interpretation software of the WinG Link 2D inversion data modeling package. Multiple homogeneous half-space initial models were tested during the 2D inversion process. The findings indicate the existence of a midcrustal conductor associated with graphites and iron sulfides in the source region. This conductivity may be attributed to processes such as exsolution of metamorphic fluids, influx of mantle sources, or the entry of magmatic fluids through transcrustal fault zones.
The findings indicate that the intrusive granite was emplaced along a NE–SW major fault, penetrating shallow crustal levels. The depth of this granite intrusion is determined to be 15 km, covering an outcrop area of 60 km². This detailed geological information allows a comprehensive assessment of the power-generating capacity of the intrusive granite. The results of this investigation contribute valuable insights for the development and optimization of Enhanced Geothermal System (EGS) projects in the region.

Key words: Kozak granite, magnetotelluric, enhanced geothermal systems, Bergama,Örenli-Eğiller depression

1. Introduction

Due to the interaction of the Arabian, African, and Eurasian plates, Western Anatolia is a seismically active continental region. While the Eurasian plate is comparatively stable, the Arabian and African plates migrate in a northerly direction. As a result, a large portion of the country moves westward, away from the area where the Arabian and Eurasian plates collide. Consequently, most of Türkiye's landmass is represented by the Anatolian block, a wedge-shaped piece of continental crust (Reilinger et al., 2006; Reilinger and McClusky, 2011). Two significant strike-slip faults, the 550 km East Anatolian Fault and the 1500 km North Anatolian Fault, which run along opposite sides of the wedge and terminate in the Aegean, respectively, are responsible for the wedge's movement (Reilinger et al., 2006; Chousianitis et al., 2015).

During the Late Oligocene–Early Miocene, Western Anatolia experienced widespread magmatism. Numerous magmatic associations, including volcanic and plutonic rocks, were formed as a result. The Triassic metapelites and metabasites comprise the metamorphic basement rocks where the Kozak pluton was emplaced (Kaya and Mostler, 1992). Around its periphery, the pluton possesses a well-developed contact aureole (İzdar, 1968). The Kozak intrusion is an oval body with a long axis that runs from the southwest to the northeast. Granodiorites and granites, which exhibit transitional contacts, are significant rocks. Under an E–W extensional regime, thick volcanic sedimentary associations evolved throughout the Early–Middle Miocene epoch within roughly N–S-trending fault-bounded continental basins (Yilmaz et al., 2000; Şahin et al., 2010). Western Anatolia's intercontinental plate alkaline volcanic province developed between the Late Miocene and Quaternary (e.g., Aldanmaz et al., 2000; Aldanmaz, 2006) after the N–S extension had commenced.

The widespread magmatism in Western Anatolia may have been caused by large-scale upwelling, partial melting, or thermal remobilization of crustal and mantle material

* Correspondence: dchandra50@gmail.com

(Schleiffarth et al., 2018; Okay et al., 2020, 2022). This might have enhanced the crustal/upper mantle conductivity and requires to be mapped by magnetotelluric (MT) methods. Three MT profiles conducted over Kozak (as shown in Figures 1a and 1b) have been measured across the Örenli-Eğiller depression to reveal the geoelectrical structure of the depression zone. The total length of the profile is about 12 km with 1-km MT station spacing.

2. Geological background

The geology of Türkiye is a combination of microcontinents placed between Gondwana and Laurasia from the Permo-Triassic until the Oligocene. During the Oligocene, western Türkiye showed N–S extensional tectonics (Seyitoğlu and Scott, 1996; Seyitoğlu et al., 2004), and then was characterized by east–west trending, subparallel, normal fault zones bordering a set of grabens and intervening horst blocks (Yilmaz et al., 2000). There are about ten east–west-orientated grabens in Western Anatolia. The study area is north of the Bergama Graben region across the Örenli-Eğiller depression zone (Figure 1b).

The Kozak Horst is the most prominent morphological feature of the region and consists of metamorphic, plutonic, volcanic, and Neogene sedimentary rocks. In the central part of the Kozak Horst, a granitic pluton was emplaced into the metamorphic rocks during the latest Oligocene–Early Miocene times (20–23 Ma; Bingöl et al., 1982). The pluton is primarily composed of coarse-grained, porphyritic diorites and is encircled by several dykes. This uplifted block, or horst, is separated from the adjacent downdropped blocks, or grabens, by a series of faults exhibiting northeast–southwest and north-northwest–south-southeast orientations. The volcanics were fed from fissures, linked with the northeast–southwest graben-bounding faults, and dated 9–6 Ma (Bozkurt et al., 2000). In the present study, three profiles extending from the Kozak granite massif to the Örenli-Eğiller grabens were analyzed to determine the geoelectrical structure between these formations.

3. Magnetotelluric data processing and interpretation

The MT system can explore the Earth's crustal shallow to deeper layers by recording its electric and magnetic field variations. MT data were acquired at 32 stations in three closely spaced profiles by FNC Engineering consultancy services (Ankara, Türkiye). Data were obtained using an MTU-5A unit manufactured by Phoenix Geophysics (Toronto, Canada). Next, time series processing was performed using the SSMT 2000 software package available with the Phoenix Geophysics system based on robust reference cascade decimation (Jones, 1983). The examination of MT data involves conducting frequency domain analysis. Cross-spectra/power spectra computations are performed between the magnetic field component Bx and the electric field component Ey, as well as between By and Ex, at various frequencies. The objective is to ascertain the impedance tensors (Zxx, Zxy, Zyx, and Zyy). Subsequently, apparent resistivity (ρ_{xx}, ρ_{xy}, ρ_{yx}, and ρ_{yy}) and phases (Φ_{xx}, Φ_{xy}, Φ_{yx}, and Φ_{yy}) are derived for different frequencies based on these impedance tensors for 0.001 to 1000 s. These curves are presented and discussed in subsection 3.3.

3.1. Dimensionality analysis

Before the inversion of MT data, it is essential to understand the dimensionality of these data to obtain subsurface measurements as well as the orientation

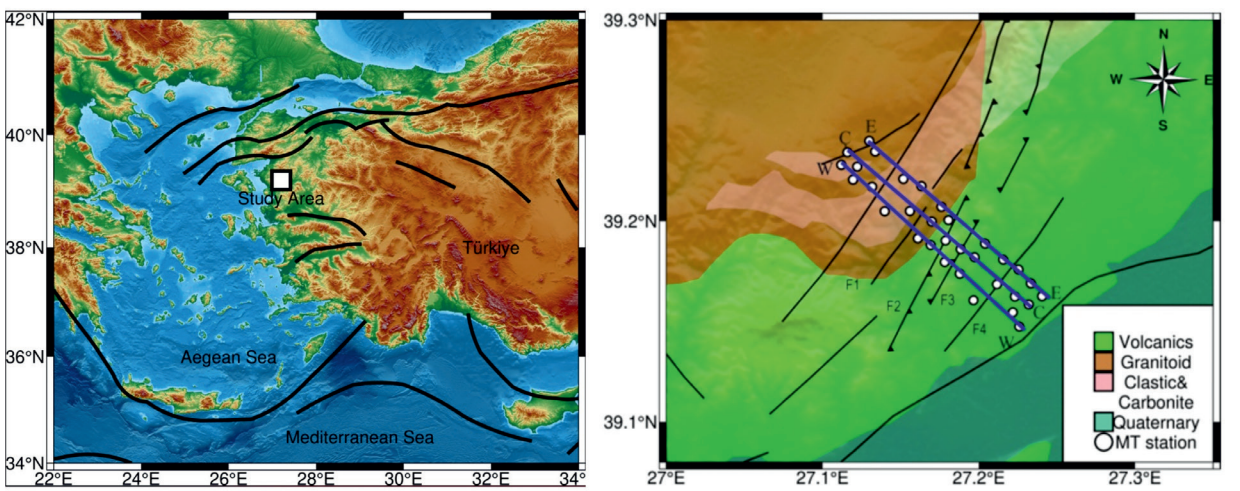

Figure 1. (a) Tectonic map of Western Anatolia (modified after Okay (2008) and Black (2012)). (b) Location map of the study area; 30 MT sites were placed across the Örenli-Eğiller depression in three different profiles. WW: western profile, CC: central profile, and EE: eastern profile.

of subsurface structures. In the present study, dimensionality analysis was performed using Bahr skew (Bahr, 1991) and phase tensor analysis (Caldwell et al., 2004).

In Bahr skew, if amplitude values are greater than 0.3, it implies that the MT data exhibit 3D behavior. Bahr skew values calculated for three profiles are shown in Figure 2. As observed therein, skew values vary from 0 to 0.3 for all stations, indicating that the structure is 1D/2D in nature up to 0.1 s. After 0.1 s, the skew values are greater than 0.3, denoting the 3D nature of the subsurface layers.

The phase tensor ellipses of all stations are shown in Figure 3. Ellipses become circles at short periods (between 0.01 and 0.1 s), and skew angles are less than ±3°, denoting the data's 1D and 2D nature. Above 0.1 s, the skew value is in the range of ±3°, representing the 3D nature of the MT data.

3.2. Strike angle

In the present study, the regional strike assessed through Groom–Bailey (GB) analysis (Groom and Bailey, 1989) suggests an N 60° E direction, as shown in Figure 4a, which coincides with the strike direction obtained in phase tensor analysis (Figure 4b). In the 2D analysis and interpretation process, we rotated the impedance tensor as N 60° E at each station. Thus, rotation of the impedance tensor allows decoupling into the transverse electric TE and transverse magnetic TM modes.

3.3. 2D inversion of MT data

The rotated impedance tensors, in conjunction with tippers, underwent inversion using the nonlinear conjugate gradient (NLCG) algorithm developed by Rodi and Mackie (2001). This inversion process was executed within the MT interpretation software integrated into the WinG Link data modeling package, which was developed by Schlumberger Limited (London, UK). The NLCG method addresses the inverse problem by employing the Tikhonov regularization parameter. This parameter is utilized to minimize an objective function, denoted as Ψ (as detailed in Rodi and Mackie (2001)). The objective is to attain the smoothest model that optimally aligns with the observed data, resulting in the best fit. NLCG provides the flexibility to select either the standard grid Laplacian (SGL) operator or the uniform grid Laplacian (UGL) operator. With the SGL operator, derivatives are computed in both the horizontal and vertical directions. On the other hand, when employing the UGL operator, the horizontal derivative remains constant, resulting in smoothening exclusively along the vertical direction. The 2D inversion was performed using different homogeneous half-space initial models; 10, 100, and 1000 Ω m were tested, and a homogeneous half-space of 100 Ω m was identified as an initial model. In the collaborative inversion model, an error threshold of 25% was designated for apparent resistivity in TE mode, 10% for apparent resistivity in TM mode, and 5% (1.45) for phase measurements in both modes. 2D

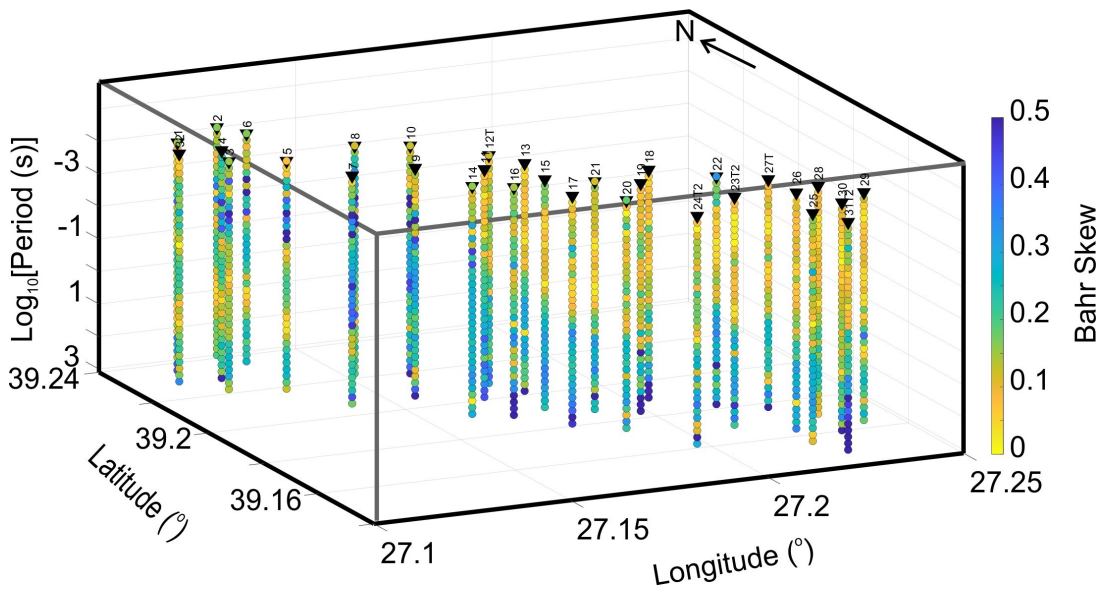

Figure 2. The Bahr's (Bahr, 1991) phase-sensitive skew plot of the Örenli-Eğiller depression zone for all stations showing 2D subsurface nature up to 100 s and 3D nature for periods greater than 100 s.

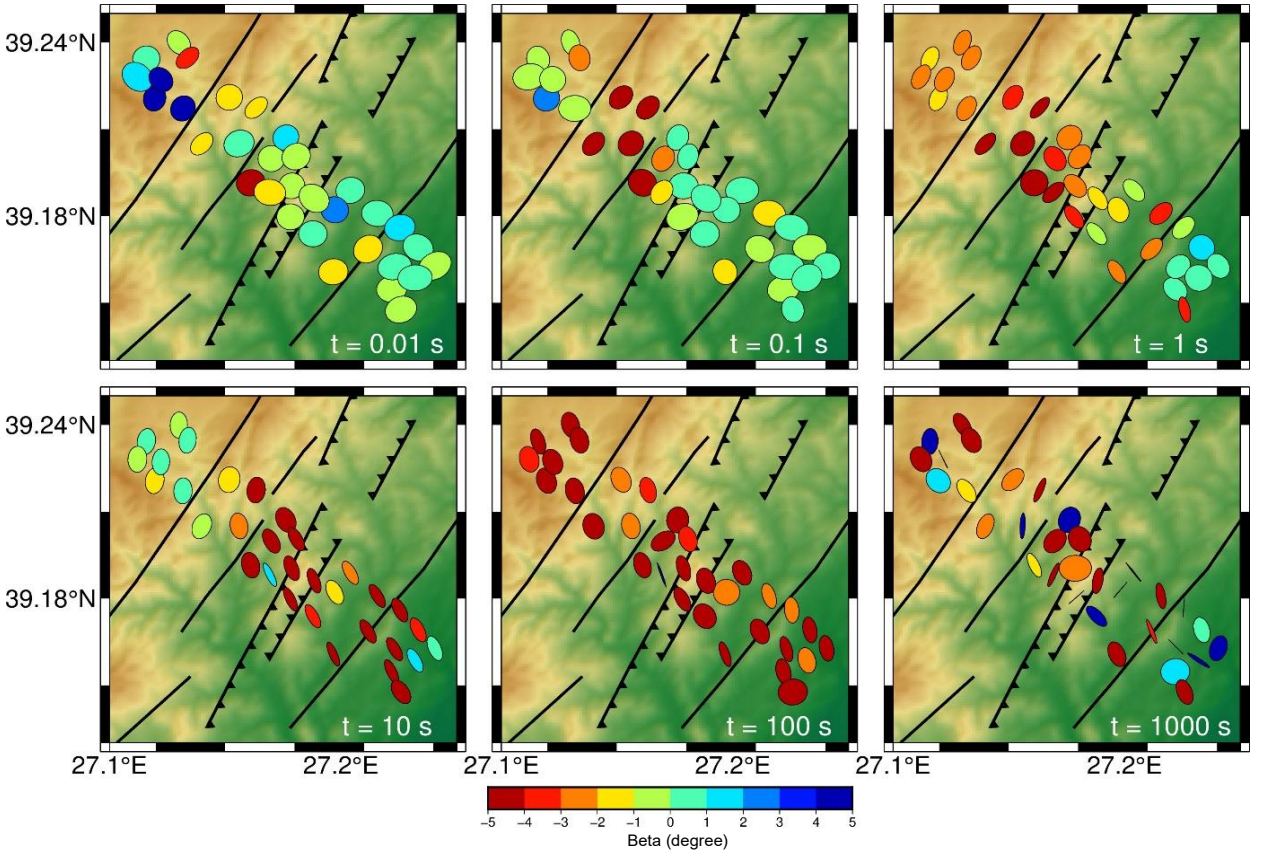

Figure 3. Phase tensor ellipses for three profiles from 0.1 to 1000 s. Major axes of the ellipses are oriented in the NE–SW direction for up to 100 s with $|\beta| \leq \pm 3$ suggesting 2D nature, which becomes 3D at higher periods.

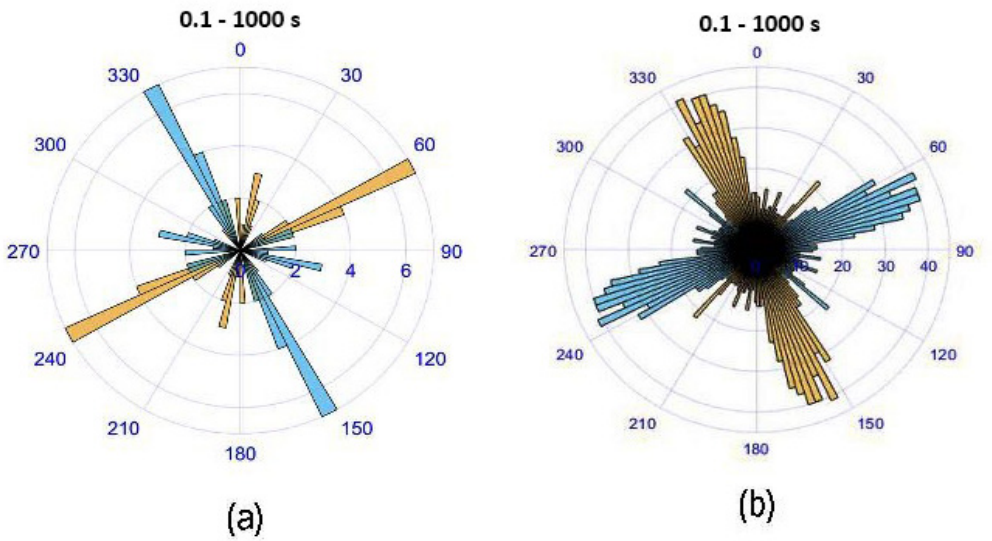

Figure 4. (a) Multifrequency rose diagram of three west–east profiles showing geoelectrical strike direction using the Groom–Bailey (Groom and Bailey, 1989) tensor decomposition technique. Regional strike obtained is about N 60° E. (b) Phase tensor strike estimate for the entire data set (0.1–1000 s) also denotes N 60° E.

inversion using a SGL operator yields better modeling results in deriving the deeper subsurface resistivity structure. The regularization parameter (τ) controls the trade-off between the RMS and model roughness. However, we can observe two extreme cases: (a) if the regularization parameter (τ) is a small value, the observed data best fit with the calculated response, but it derives a rough, even unpredictable resistivity structure, (b) if the regularization parameter (τ) is an enormous value, it derives a smooth model but with inadequate fit between observed and calculated response. The mesh of 60 × 101 (rows and columns) was used to generate the L-curves for three different profiles, as shown in Figure 5. For selecting the τ, the inversion was performed with 200 iterations by varying different τ values such as 1, 2, 3, 5, 7, 10, 15, 20, 50, and 100. The value of τ = 5 is considered for the final model in three different profiles. After 160 iterations, there was no significant change in the RMS value and hence the inversion stopped. The absolute RMS error was between 2.3 and 2.4 for the last iteration. The last 2D resistivity cross section was obtained using TE and TM mode data as shown in Figures 6a–6c. The observed and calculated apparent resistivity and phase pseudosections for west, central, and east profiles are shown in Figures 7a–7c.

4. Sensitivity analysis

The current MT dataset underwent depth derivation using the Niblett–Bostick method (Bostick, 1977; Jones, 1983) for TE and TM modes separately. The objective was to determine the maximum penetration depth of the data, as illustrated in Figure 8. A depth of 20 km was chosen, revealing a uniform penetration depth across all sites.

Before drawing any conclusions, the geoelectrical model resulting from the inversion of MT data in both TE and TM modes undergoes thorough sensitivity analysis, as outlined by Brasse et al. (2002) and Ledo et al. (2004). The primary objective of this analysis is to assess the reliability and stability of the identified subsurface features.

In this particular investigation, the sensitivity test is executed by masking the conductivity anomaly obtained along the three profiles with a resistivity value of surrounding formations (as shown in Figures 9–11) and then restarting inversion. Forward and inversion modeling is conducted to analyze the modified model depicted in Figure 11c. The RMS error obtained in the forward model is approximately 18.0 to 22.0. Different conductivity features in the three different models reappeared after inversion, indicating the existence of conductive features. Consequently, the inclusion of conductive elements, as illustrated in models in Figures 9–11, becomes necessary to elucidate the observed TE and TM mode datasets.

The 2D inversion models underwent rigorous sensitivity analysis following the method proposed by Rodi and Mackie (2001). This approach involves transforming the data into the logarithm of complex apparent resistivity and the model into the logarithm of resistivity. The sensitivity matrix thus obtained captures how changes in the logarithm of resistivity affect the logarithm of complex apparent resistivity in the data.

Each sensitivity matrix comprises real values, with consecutive rows representing the real and imaginary parts of the dataset. By summing the squares of each column across all data points (stations and frequencies), one obtains a measure of sensitivity. In the present study,

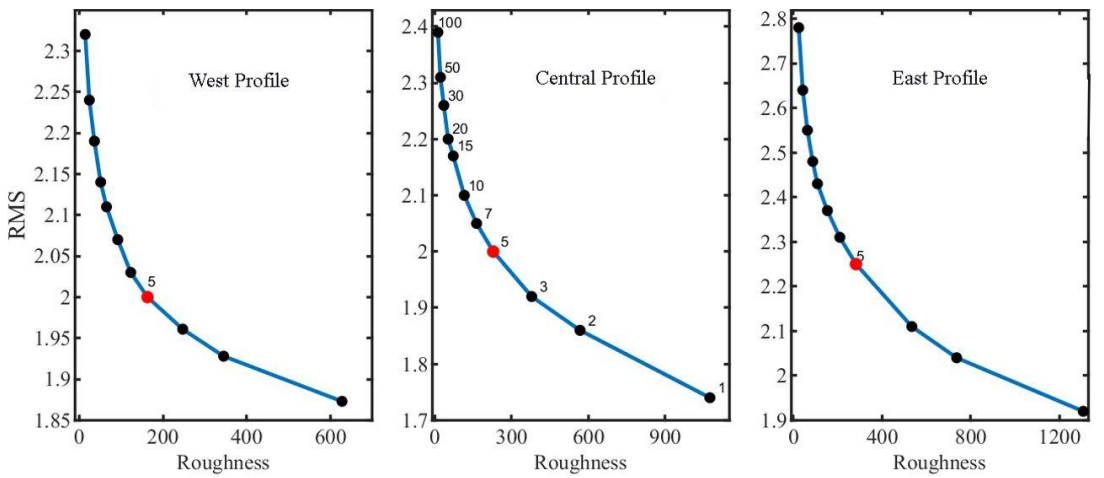

Figure 5. RMS error versus roughness (L-curve) plot for (a) west, (b) central, and (c) east profiles. The circles mark the RMS misfit and roughness values for a range of tau (1, 2, 3, 5, 7, 10, 15, 20, 30, 50, and 100). The corner point of the curve (marked by the red circle) represents an optimal trade-off between data misfit and model roughness. For example, the corner point of the curve for the profiles corresponds to a value of $\tau = 5$, which represents a balanced weighting of data misfit and model roughness at the same time.

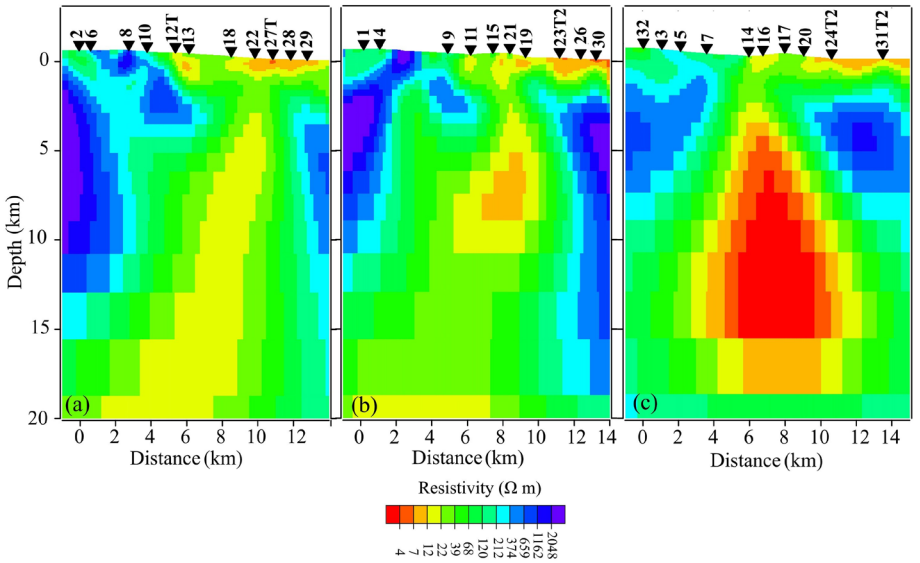

Figure 6. The geoelectric structure beneath the Örenli-Eğiller depression for (a) west, (b) central, and (c) east profiles is reflected as a high conductivity anomaly along the fault/fracture zone related to an accumulation of fluids (source region for mineralized zones) at midcrustal depths, and the shallow conductivity anomaly could be related to the mineralized zones trapped beneath an impermeable layer, and it increases towards the east.

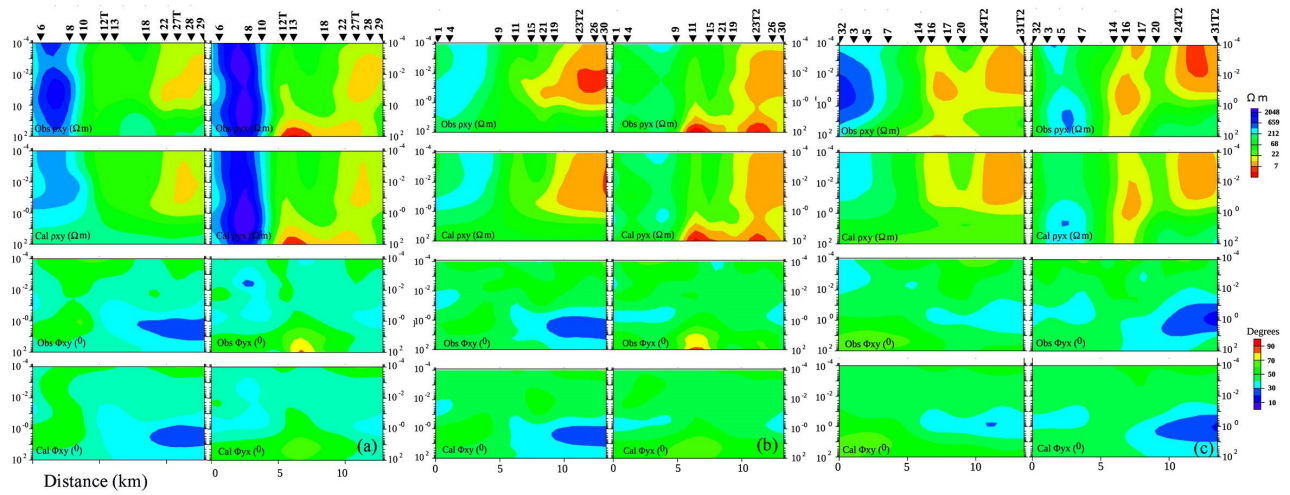

Figure 7. Pseudosections for observed and computed TE and TM mode data along the (a) west, (b) central, and (c) east profiles.

structures with sensitivity matrix values exceeding 0.0001 were considered resolved features, aligning with similar findings by other researchers such as Brasse et al. (2002), Ledo et al. (2004), Newman and Alumbaugh (2000), Demirci et al. (2012), and Özyıldırım et al. (2017).

Furthermore, sensitivity maps were generated for the 2D models across all profiles (Figure 12). These maps reveal lower sensitivity values over highly resistive structures. Notably, the models highlight a significant conductive anomaly in the upper–lower crust along the three profiles, exhibiting sensitivity ranging from 0.05 to 1.24. For instance, the western profile illustrates a conductivity anomaly beneath stations 13–29, extending from surface to depth, strongly supported by high sensitivity values in Figure 12 (left panel). Similarly, the central profile (between stations 9 and 19) shows correlation between high conductivity anomalies and sensitivity in the 5–10 km depth range (Figure 12, central panel). The eastern profile also exhibits high sensitivity values in the 5–10 km depth beneath stations 7–17 (Figure 12, right panel).

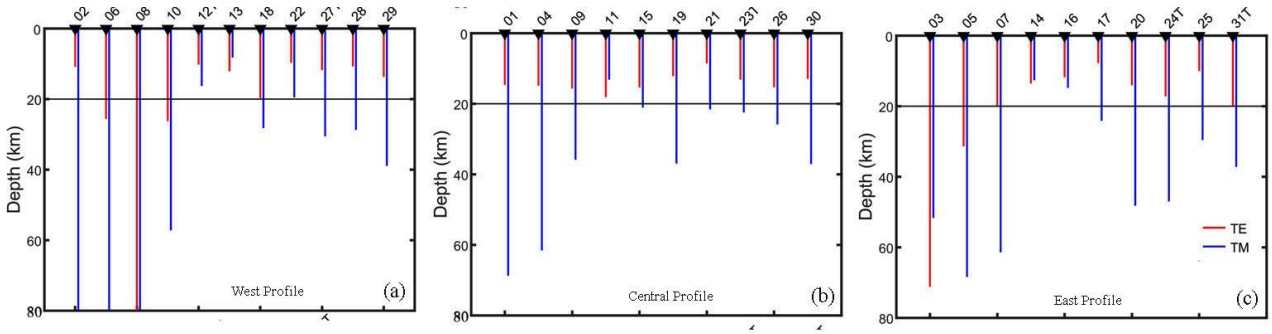

Figure 8. Niblett–Bostick depth for three profiles. Red and blue solid lines represent TE and TM data, respectively. In the present study, we adopted up to a depth 20 km as shown in the figure.

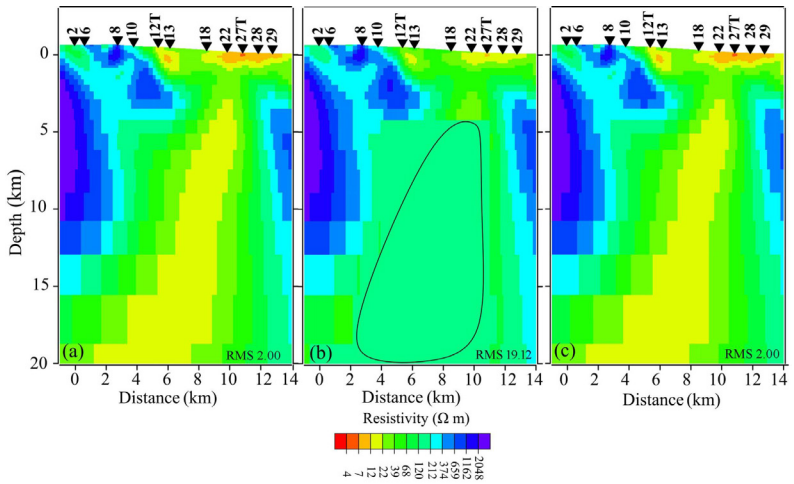

Figure 9. (a) Sensitive analyses are carried out for MT stations along the western profile. This is done by masking the midcrustal conductor below 12, 13, 18, 22, and 27 T sites. (b) The RMS fit before constrained inversion and (c) RMS misfit after constrained inversion.

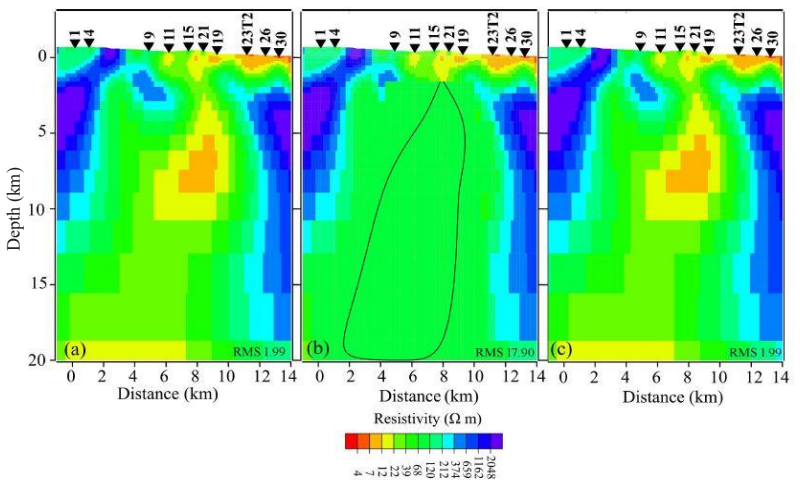

Figure 10. (a) Sensitive analyses are carried out for MT stations along the central profile. This is done by masking the midcrustal conductor below 9, 11, 15, 21, and 19 sites. (b) The RMS fit before constrained inversion and (c) RMS misfit after constrained inversion.

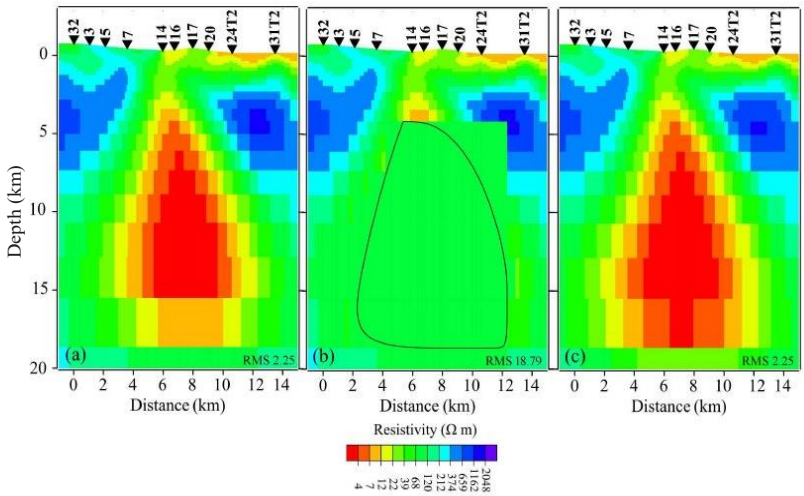

Figure 11. (a) Sensitive analyses are carried out for MT stations along the eastern profile. This is done by masking the midcrustal conductor below 14, 16, 17, 20, and 24 T sites. (b) The RMS fit before constrained inversion and (c) RMS misfit after constrained inversion.

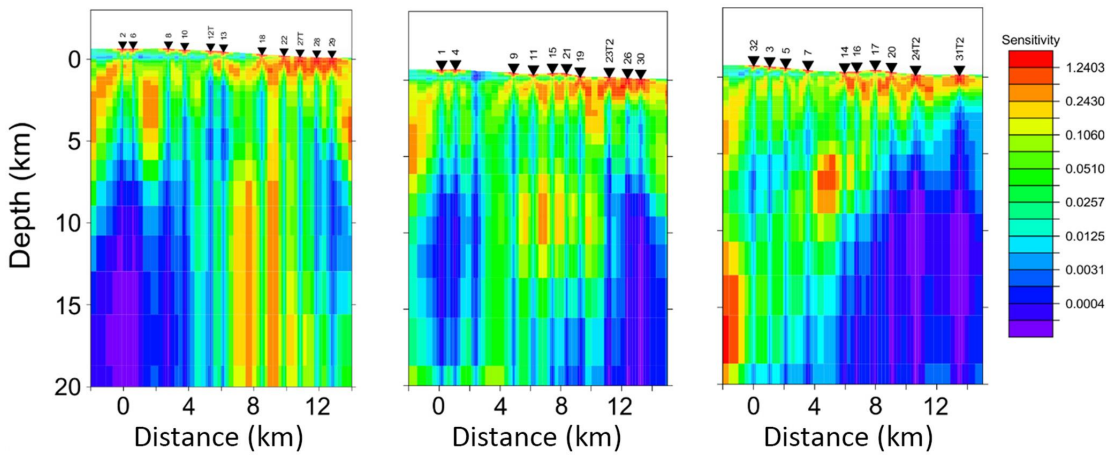

Figure 12. Sensitivity map of 2D features in the study area; the robustness of high conductive features is shown with high sensitivity values in the plot.

These findings underscore distinct conductive features in the upper–lower crust across the three profiles, enhancing clarity and visibility in the models.

5. Results and discussion

Black (2012) and Black et al. (2013) suggested that dehydration of the Anatolide-Tauride Block's subducting slab triggered two significant events: the melting of the mantle fluid stream and partial melting within the overlying Sakarya and Rhodope zones. These processes are thought to have given rise to the granitic magmas observed at the Kozak (Bergama Region) and Kestanbolu (Biga Peninsulla) plutons. Geochemistry studies suggest that these plutons have had multiple magma injections at different periods (Black et al., 2013). During Eocene times, the collision between the Anatolide-Tauride Block and the Sakarya Zone occurred along the İAESZ (Harris et al., 1994). During this period, upward doming and movement of the larger magma body through the crust may have contributed to the exhumation of the Kozak pluton. The earlier-mentioned process and the partial melting of the overlying mantle wedge might have generated these magmas due to large-scale extension during the Late Oligocene to the Early Miocene.

The subduction of the oceanic lithosphere of the African plate and the overriding Eurasian plate led to the extension of the Aegean (Brun and Faccenna; 2008, Brun and Sokoutis, 2007, 2010). Due to this process, different

grabens have developed in western Türkiye (Altunkaynak and Yılmaz, 1998; Yilmaz et al., 2000; Şahin et al., 2010). For example, the Bergama Graben is located south of the Kozak pluton with active normal faults (having NE–SW trend) bounded by the graben. The Örenli-Eğiller depression zone is situated between the Kozak pluton and the Bergama Graben, extending in an NE–SW direction.

Most of the Örenli-Eğiller depression zone is filled with volcanic products. In MT profiles, an anomalous conductivity zone is reflected between fault zones F1 and F4, as shown in Figure 1. It appears as a deep-seated fracture/fault zone extending to the base of the crust (Moho), which may have facilitated magma spreading both vertically as well as horizontally. The source of the magma could be the partial melting of the subduction African plate and the overlying crust of the Eurasian plate. Conductivity at deeper levels could be related to the partial melting of the lithosphere, and the addition of magma at the base of the crust can take place in the form of a sequence of sills that get differentiated into gabbroic and ultramafic rocks at the upper and lower levels. Thus, the trapped magma at the base of the crust propagates to shallow levels due to the exchange of heat with the lower crust. Hot magma induces partial melting, releases large amounts of H_2O and CO_2 fluids upon crystallization, and contributes to shallow conductivity anomalies. High resistive bodies correspond to granites in the study area. The average thickness of the granites along this traverse is about 15 km.

During extensional forces in the N–S direction (Dewey and Şengör, 1979; Bozkurt et al., 2000; Bozkurt, 2001), upward doming and movement of the larger magma bodies (partial melting material) through the crust (Western Anatolia) may have occurred through fault zones F1 and F4 as shown in Figure 1. Thus, linear conductivity zones along the three profiles may be related to dehydration of minerals during contact metamorphism of the intrusive with the country rocks at deeper depths (Byerlee, 1993). The most plausible sources for orogenic gold deposits, supported by geochemical evidence, involve the exsolution of metamorphic fluids, contributions from mantle sources, or the infiltration of magmatic fluids through transcrustal fault zones (F1–F4, Goldfarb and Groves, 2015). The midcrustal irregularities may result from the combination of graphites and iron sulfides within the source region, as suggested by Heinson et al. (2021). This conductivity zone increases as one moves from west to east.

These data can be used to determine the depth of the Kozak intrusive, which is essential to estimate the volume of the pluton and assess the quantity of heat that can be captured from this granite. From the field investigations, this elliptical pluton with a surface outcrop of 60 km^2, as evident from the present study, extends to lower crustal levels. A conservative estimate of a minimum of 900 km^3 can be assumed for this pluton. A 3D analysis of the MT results is being carried out to estimate the real volume of this pluton. Until such time, based on the earlier studies carried out on similar granites of Western Anatolia (Chandrasekharam et al., 2023), the Kozak pluton can generate a minimum of 71×10^9 kWh of electricity. This amount will be refined once the 3D MT model for Kozak granite is developed.

6. Conclusion

MT studies across the Örenli-Eğiller depression zone reveal three linear conductivity zones. These zones are related to volcanic eruptions that spread horizontally and vertically up to the surface. This volcanic phase was preceded by the intrusive activity represented by a granite body with a thickness of 15 km below the MT traverse site. Both volcanic and intrusive magmatic activities are associated with subduction-related tectonism of the African plate. This investigation is an important contribution to determining the magnitude of depth and the volume of the granite pluton in this region. A conservative volume of 900 km^3 of Kozak granite can generate 71×10^9 kWh of electricity.

Acknowledgments

The MT field investigation was supported by The Scientific and Technological Research Council of Türkiye (TÜBİTAK) (project no: 120C079). KR's research was supported by PNRR-RETURN project funding from the European Union's Next Generation EU fund. We express our gratitude to Tolga Ayzit for his invaluable support in the field.

Conflict of interest

The authors declare that they have no conflict of interest.

Funding

This work did not receive any financial support from a funding agency.

References

Aldanmaz E, Pearce JA, Thirlwall M, Mitchell JG (2000). Petrogenetic evolution of late Cenozoic, post-collision volcanism in western Anatolia, Turkey. Journal of Volcanology and Geothermal Research 102 (1-2): 67-95. https://doi.org/10.1016/S0377-0273(00)00182-7

Aldanmaz E (2006). Mineral-chemical constraints on the Miocene calc-alkaline and shoshonitic volcanic rocks of Western Turkey: disequilibrium phenocryst assemblages as indicators of magma storage and mixing conditions. Turkish Journal of Earth Science 15 (1): 47-73.

Altunkaynak Ş, Yılmaz Y (1998). The Mount Kozak magmatic complex, western Anatolia. Journal of Volcanology and Geothermal Research 85 (1-4): 211-231. https://doi.org/10.1016/S0377-0273(98)00056-0

Bahr K (1991). Geological noise in magnetotelluric data: a classification of distortion types. Physics of the Earth and Planetary Interiors 66 (1-2): 24-38. https://doi.org/10.1016/0031-9201(91)90101-M

Bingöl E, Delaloye M, Ataman G (1982). Granitic intrusions in western Anatolia: a contribution to the geodynamic study of this area. Eclogae Geologicae Helvetiae 75: 437-446. https://doi.org/10.5169/seals-165237

Black KN (2012). Geochemical and geochronological relationships between granitoid plutons of the Biga Peninsula, NW Turkey. M.Sc. Thesis, University of Texas, Austin, TX, USA.

Black KN, Catlos EJ, Oyman T, Demirbilek M (2013). Timing Aegean extension: evidence from *in situ* U–Pb geochronology and cathodoluminescence imaging of granitoids from NW Turkey. Lithos 180-181: 92-108. https://doi.org/10.1016/j.lithos.2013.09.001

Bostick FX (1977). A simple almost exact method of MT analysis. Workshop on Electrical Methods in Geothermal Exploration U.S. Geological Survey, Contract 14080001-8, volume 359. Reston, VA, USA: U.S. Geological Survey, pp. 174-183.

Bozkurt E, Winchester JA, Piper JDA (2000). Tectonics and magmatism in Turkey and surrounding area. Geological Society of London, Special Publication 173: 450.

Bozkurt E (2001). Neotectonics of Turkey – a synthesis. Geodinamica Acta 14 (1-3): 3-30. https://doi.org/10.1080/09853111.2001.11432432

Brasse H, Lezaeta P, Rath V, Schwalenberg K, Soyer W et al. (2002). The Bolivian Altiplano conductivity anomaly. Journal of Geophysical Research 107 (B5): EPM4-1–EPM4-14. https://doi.org/10.1029/2001JB000391

Brun J-P, Faccenna C (2008). Exhumation of high-pressure rocks driven by slab rollback. Earth and Planetary Science Letters 272 (1-2): 1-7. https://doi.org/10.1016/j.epsl.2008.02.038

Brun J-P, Sokoutis D (2007). Kinematics of the Southern Rhodope Core Complex (North Greece). International Journal of Earth Sciences 96 (6): 1079-1099. https://doi.org/10.1007/s00531-007-0174-2

Brun J-P, Sokoutis D (2010). 45 m.y. of Aegean crust and mantle flow driven by trench retreat. Geology 38 (9): 815-818. https://doi.org/10.1130/G30950.1

Byerlee J (1993). Model for episodic flow of high-pressure water in fault zones before earthquakes. Geology 21 (4): 303-306. https://doi.org/10.1130/0091-7613(1993)021<0303:MFEFOH>2.3.CO;2

Caldwell TG, Bibby HM, Brown C (2004). The magnetotelluric phase tensor. Geophysical Journal International 158 (2): 457-469. https://doi.org/10.1111/j.1365-246X.2004.02281.x

Chandrasekharam D, Baba A, Ayzit T (2023). High radiogenic granites of western Anatolia for EGS. In: Chandrasekharam D and Baba A (editors). Enhanced Geothermal Ssytems (EGS): The Future Energy Road Ahead. Oxfordshire, UK: CRC Press, p. 224.

Chousianitis K, Ganas A, Evangelidis CP (2015). Strain and rotation rate patterns of mainland Greece from continuous GPS data and comparison between seismic and geodetic moment release. Journal of Geophysical Research, Solid Earth 120 (5): 3909-3931. https://doi.org/10.1002/2014JB011762

Demirci I, Erdoğan E, Candansayar ME (2012). Two-dimensional inversion of direct current resistivity data incorporating topography by using finite difference techniques with triangle cells: investigation of Kera fault zone in western Crete. Geophysics 77: E67-E70. https://doi.org/10.1190/geo2011-0130.1

Dewey JF, Şengör AMC (1979). Aegean and surrounding regions: complex multiplate and continuum tectonics in a convergent zone. Geological Society of America Bulletin 90 (1): 84-92. https://doi.org/10.1130/0016-7606(1979)90<84:AASRCM>2.0.CO;2

Goldfarb RJ, Groves DI (2015). Orogenic gold: common or evolving fluid and metal sources through time. Lithos 233: 2-26. https://doi.org/10.1016/j.lithos.2015.07.011

Groom RW, Bailey RC (1989). Decomposition of magnetotelluric impedance tensors in the presence of local three-dimensional galvanic distortion. Journal of Geophysical Research 94 (B2): 1913-1925. https://doi.org/10.1029/JB094iB02p01913

Harris NBW, Kelley S, Okay AI (1994). Post-collisional magmatism and tectonics in northwest Anatolia. Contributions to Mineralogy and Petrology 117: 241-252. https://doi.org/10.1007/BF00310866

Heinson G, Duan J, Kirkby A, Robertson K, Thiel S et al. (2021). Lower crustal resistivity signature of an orogenic gold system. Scientific Reports 11: 15807. https://doi.org/10.1038/s41598-021-94531-8

İzdar KE (1968). Petrology of the Kozak intrusive massif and its geologic relations with the Paleozoic surrounding rocks. Geology Bulletin of Türkiye 11: 140-179 (in Turkish).

Jones AG (1983). On the equivalence of the "Niblett" and "Bostick" transformations in the magnetotelluric method. Journal of Geophysics 53 (1): 72-73.

Kaya O, Mostler H (1992). A Middle Triassic age for low-grade greenschist facies metamorphic sequence in Bergama (Izmir), western Turkey: the first paleontological age assignment and structural-stratigraphic implications. Newsletters on Stratigraphy 26 (1): 1-17. https://doi.org/10.1127/nos/26/1992/1

Ledo J, Jones AG, Ferguson IJ, Wolynec L (2004). Lithospheric structure of the Yukon, northern Canadian Cordillera, obtained from magnetotelluric data. Journal of Geophysical Research 109 (B4). https://doi.org/10.1029/2003jb002516

Newman GA, Alumbaugh DL (2000). Three-dimensional magnetotelluric inversion using non-linear conjugate gradients. Geophysical Journal International 140 (2): 410-424. https://doi.org/10.1046/j.1365-246x.2000.00007.x

Okay AI (2008). Geology of Turkey: a synopsis. Anschnitt 21: 19-42.

Okay AI, Zattin M, Özcan E, Sunal G (2020). Uplift of Anatolia. Turkish Journal of Earth Sciences 29 (5): 696-713. https://doi.org/10.3906/yer-2003-10

Okay AI, Topuz G, Kylander-Clark ARC, Sherlock S, Zattin M (2022). Late Paleocene – Middle Eocene magmatic flare-up in western Anatolia. Lithos 428-429: 106816. https://doi.org/10.1016/j.lithos.2022.106816

Özyıldırım Ö, Candansayar ME, Demirci İ, Tezkan B (2017). Two-dimensional inversion of magnetotelluric/radiomagnetotelluric data by using unstructured mesh. Geophysics 82 (4): E197-E210. https://doi.org/10.1190/geo2016-0378.1

Schleiffarth WK, Darin MH, Reid MR, Umhoefer PJ (2018). Dynamics of episodic Late Cretaceous–Cenozoic magmatism across Central to Eastern Anatolia: new insights from an extensive geochronology compilation. Geosphere 14 (5): 1990-2008. https://doi.org/10.1130/GES01647.1

Seyitoğlu G, Scott BC (1996). Age of the Alaşehir graben (west Turkey) and its tectonic implications. Geological Journal 31 (1): 1-11. https://doi.org/10.1002/(SICI)1099-1034(199603)31:1<1::AID-GJ688>3.0.CO;2-S

Seyitoğlu G, Işık V, Çemen İ (2004). Complete Tertiary exhumation history of the Menderes Massif, western Turkey: an alternative working hypothesis. Terra Nova 16 (6): 358-364. https://doi.oeg/10.1111/j.1365-3121.2004.00574.x

Rodi W, Mackie RL (2001). Nonlinear conjugate gradients algorithm for 2-D magnetotelluric inversion. Geophysics 66: 174-187. https://doi.org/10.1190/1.1444893

Reilinger R, McClusky S, Vernant P, Lawrence S, Ergintav S et al. (2006). GPS constraints on continental deformation in the Africa-Arabia- Eurasia continental collision zone and implications for the dynamics of plate interactions. Journal of Geophysical Research 111 (B5): B05411. https://doi.org/10.1029/2005JB004051

Reilinger R, McClusky S (2011). Nubia–Arabia–Eurasia plate motions and the dynamics of Mediterranean and Middle East tectonics. Geophysics Journal International 186 (3): 971-979. https://doi.org/10.1111/j.1365-246X.2011.05133.x

Yilmaz Y, Genç ŞC, Gürer F, Bozcu M, Yilmaz K et al. (2000). When did the western Anatolian grabens begin to develop? Geological Society, London, Special Publications 173: 353-384. https://doi.org/10.1144/GSL.SP.2000.173.01.17

Şahin SY, Örgün Y, Güngör Y, Göker AF, Gültekin AH et al. (2010). Mineral and whole-rock geochemistry of the Kestanbol Granitoid (Ezine-Çanakkale) and its mafic microgranular enclaves in northwestern Anatolia: evidence of Felsic and Mafic Magma Interaction. Turkish Journal of Earth Sciences 19 (1): 101-122. https://doi.org/10.3906/yer-0809-3